

# Complexity of Gaussian boson sampling with tensor networks

Minzhao Liu,<sup>1,2</sup> Changhun Oh,<sup>3</sup> Junyu Liu,<sup>3,4,5,6,7,8</sup> Liang Jiang,<sup>3,5</sup> and Yuri Alexeev<sup>2,4,5</sup>

<sup>1</sup>*Department of Physics, The University of Chicago, Chicago, IL 60637, USA*

<sup>2</sup>*Computational Science Division, Argonne National Laboratory, Lemont, IL 60439, USA*

<sup>3</sup>*Pritzker School of Molecular Engineering, The University of Chicago, Chicago, IL 60637, USA*

<sup>4</sup>*Department of Computer Science, The University of Chicago, Chicago, IL 60637, USA*

<sup>5</sup>*Chicago Quantum Exchange, Chicago, IL 60637, USA*

<sup>6</sup>*Kadanoff Center for Theoretical Physics, The University of Chicago, Chicago, IL 60637, USA*

<sup>7</sup>*qBraid Co., Chicago, IL 60615, USA*

<sup>8</sup>*SeQure, Chicago, IL 60615, USA*

**Gaussian boson sampling, a computational model that is widely believed to admit quantum supremacy, has already been experimentally demonstrated and is claimed to surpass the classical simulation capabilities of even the most powerful supercomputers today. However, whether the current approach limited by photon loss and noise in such experiments prescribes a scalable path to quantum advantage is an open question. To understand the effect of photon loss on the scalability of Gaussian boson sampling, we analytically derive the asymptotic operator entanglement entropy scaling, which relates to the simulation complexity. As a result, we observe that efficient tensor network simulations are likely possible under the  $N_{\text{out}} \propto \sqrt{N}$  scaling of the number of surviving photons in the number of input photons. We numerically verify this result using a tensor network algorithm with  $U(1)$  symmetry, and overcome previous challenges due to the large local Hilbert space dimensions in Gaussian boson sampling with hardware acceleration. Additionally, we observe that increasing the photon number through larger squeezing does not increase the entanglement entropy significantly. Finally, we numerically find the bond dimension necessary for fixed accuracy simulations, providing more direct evidence for the complexity of tensor networks.**

## I. INTRODUCTION

Exact classical simulations of quantum systems are intractable due to the exponential size of the Hilbert space. As a result, computations using quantum systems have been proposed to achieve improvement in algorithmic complexities in tasks such as integer factoring [1], unstructured search [2], linear algebra [3], Hamiltonian simulations [4–7], and more [8]. Present-day quantum computational devices, however, are susceptible to noise and cannot be perfectly controlled. As a result, numerous approaches based on sampling outputs of randomly configured devices have been proposed to demonstrate quantum supremacy, which are especially appealing considering near-term constraints. For example, boson sampling [9], a process of sampling the photon output patterns from interferometers, has resulted in numerous experimental demonstrations of quantum supremacy [10–28].

However, experimental imperfections such as photon loss can have implications on the computational complexity. The

effects of noise are already examined in various contexts of quantum computing experiments. For qubits cases, it has long been known that without error correction, a quantum state after a large depth with a constant level of depolarizing noise becomes very close to the maximally mixed state [29], which enables an efficient approximate simulation. One proxy of classical simulation complexity is the entanglement entropy (EE). For pure state simulations, the computational cost using tensor networks is exponential in the EE of the quantum system, which implies that systems with logarithmic growth in the EE can be efficiently simulated. Similarly, it has been argued that the density operator EE of mixed states implies a similar computational cost, albeit some nuances [30–32]. In the context of noisy random circuit sampling (RCS) [33], it was numerically shown that the density operator EE decreases if the circuit depth is too high for 1D [30] and 2D [31] systems. Further, the maximum achievable EE follows area law scaling, suggesting the possibility of efficient tensor network simulation. More recently, polynomial time simulation of RCS with constant depolarizing noise per gate is proven to be possible in an asymptotic regime for larger than logarithmic depths, denying the scalability of RCS [34].

Meanwhile, in the context of boson sampling, a similar study has very recently shown that for a particular noise, which may not be experimentally relevant, there is an efficient classical algorithm for noisy boson sampling in an asymptotic regime [35]. Thus, the experimental noise might prohibit scalable quantum advantage in boson sampling, much like in RCS. However, it still remains possible for noisy boson sampling to be scalable under realistic noises, such as photon loss [36–39] and partial distinguishability [38, 40–43]. Notably, the effects of photon loss are investigated in several studies. For single-photon [36, 37] and gaussian boson sampling [39], when  $N_{\text{out}} \propto \sqrt{N}$  photons survive before measurement, classical state approximation of the output state provides an efficient method of simulation. However, the approximation error of these methods is fixed for given parameters and cannot be controlled with more resources. As a result, quantum supremacy intermediate-size experiments, where transmission is not as low as these approximate algorithms require, elude these methods.

Tensor network methods, on the other hand, allow us to control the simulation error by tuning time and memory resources, and have been used to numerically show the logarithmic scaling of the operator EE when  $N_{\text{out}} \propto \sqrt{N}$  in single photon boson sampling (SPBS) [32]. However, the probabilistic na-

ture of single-photon generation renders SPBS unscalable, and the community has long moved onto other photon sources [44–46]. The most promising approach is gaussian boson sampling (GBS), where no post-selection is necessary and classical simulation is hard unless some plausible complexity-theoretic conjectures are false [47, 48]. This allowed recent experimental demonstrations of GBS to claim quantum supremacy [27, 28, 49].

In this work, we investigate the operator EE scaling of GBS, which is more experimentally relevant. We show analytically that in the asymptotic limit of large  $N$ , the logarithmic operator EE scaling holds for  $N_{\text{out}} \propto \sqrt{N}$ . For numerical verification, simulation of GBS is especially difficult with tensor networks due to the infinite-dimensional local Hilbert space for each squeezed mode, which remains high even under suitable truncation and leads to dramatically increased computational cost. As a result, we develop a hardware-accelerated, supercomputing tensor network algorithm that exploits  $U(1)$  symmetry, allowing us to simulate previously intractable systems such as GBS [50]. We numerically verify the operator EE scaling of GBS under various loss conditions against the asymptotic estimates, and further observe that increasing the photon number through higher squeezing has little impact on EE. Finally, we explicitly calculate the bond dimension and the computational cost as the most direct evidence on the complexity. Overall, our work suggests that boson sampling with loss higher than the aforementioned scaling may be efficiently simulated with tensor networks as the system size grows.

## II. METHOD

Lossless and lossy quantum states in boson sampling can be represented by matrix product states (MPSs) and matrix product operators (MPOs) [32, 51]. More explicitly, given an  $M$ -body pure state

$$|\Psi\rangle = \sum_{i_1, \dots, i_M=0}^{d-1} c_{i_1, \dots, i_M} |i_1, \dots, i_M\rangle, \quad (1)$$

the corresponding MPS is

$$c_{i_1, \dots, i_M} = \sum_{\alpha_0, \dots, \alpha_M=0}^{\chi-1} \Gamma_{\alpha_0 \alpha_1}^{[1]i_1} \lambda_{\alpha_1}^{[1]} \Gamma_{\alpha_1 \alpha_2}^{[2]i_2} \lambda_{\alpha_2}^{[2]} \times \dots \lambda_{\alpha_{M-1}}^{[M-1]} \Gamma_{\alpha_{M-1} \alpha_M}^{[M]i_M}, \quad (2)$$

where  $d$  is the local Hilbert space dimension and  $\chi$  is the bond dimension. The tensor  $c_{i_1, \dots, i_M}$  fully characterizes the state  $|\Psi\rangle$  but is  $M$  dimensional, leading to  $M^d$  entries in storage. The MPS, however, represents this large tensor as a contraction (sum over the dummy or virtual  $\alpha$  indices) of a chain of tensors. One can observe that the  $i$  indices representing the physical degrees of freedom remain open (unsummed). The memory complexity of the MPS is  $O(\chi^2 d M)$ , and  $\chi$  can be adjusted to represent  $c$  with the desired accuracy. Further, one can efficiently perform local unitary operations on the MPS

and calculate expectation values of local observables with complexity  $O(d^4 \chi^3)$ .

Lossy boson sampling can be simulated using an MPO, which is essentially an MPS with additional dual indices. Time evolving the MPO can be accomplished by contracting it with Kraus operators. Further, in the case where loss is uniform, all losses can be moved to the initial state since loss commutes with linear optical transformations. As a result, full Kraus operator-based simulation of noisy channels is not necessary. We can vectorize the MPO, build a tensor network analogous to Eq. 2, and update the MPO by contracting it with unitaries [51–53].

For lossless, pure state systems with large local dimensions  $d$ , the  $O(d^4 \chi^3)$  computational complexity becomes significant. For lossy, mixed state simulations with MPOs, the complexity becomes  $O(d^8 \chi^3)$ , which is especially problematic for systems with large  $d$  such as GBS. Fortunately, for systems with global symmetry, such as particle number or total spin conservation, another level of reduction is possible. Symmetry preserving operators can be expressed as a direct sum  $\hat{T} = \bigoplus_n \hat{T}_n$  where  $\hat{T}_n$  preserves the subspace  $\mathbb{V}_n$  corresponding to some conserved charge  $n$ , and tensors can be therefore written in a block diagonal form and stored efficiently [52]. Computations are performed on different blocks independently, and the time cost also reduces due to the non-linear polynomial complexity.

The MPS formulation is especially convenient for quantifying entanglement. If we perform the Schmidt decomposition on the quantum state, which is to express the wavefunction as the sum of tensor products of states of two subsystems  $A$  and  $B$

$$|\Psi\rangle = \sum_{\alpha} \lambda_{\alpha} |\alpha_A\rangle |\alpha_B\rangle, \quad (3)$$

where  $\{|\alpha\rangle\}$  forms a basis set for each subsystem, we reveal the entanglement between the two subsystems, and the entanglement entropy (EE) given by

$$- \sum_{\alpha} \lambda_{\alpha}^2 \log \lambda_{\alpha}^2 \quad (4)$$

quantifies how much entanglement there is. Conveniently, if the subsystems are bipartitions of the MPS at site  $\ell$ , the Schmidt decomposition singular values  $\lambda_{\alpha}$ 's would be the MPS singular values  $\lambda_{\alpha_{\ell}}^{[\ell]}$ , allowing us to compute the MPS EE. For a mixed state represented by a vectorized MPO, we can formally perform Schmidt decomposition, identify the singular values  $\lambda_{\alpha}$  with  $\lambda_{\alpha_{\ell}}^{[\ell]}$  of the MPO, and similarly compute the MPO EE. In both cases, higher EE means more uniformly distributed singular values, and truncation leads to a higher approximation error. Larger bond dimensions are necessary to simulate systems with larger EE to fixed accuracy.

### III. RESULTS

#### A. Asymptotic MPO entanglement entropy scaling for boson sampling

In this section, we discuss the derivation of the operator EE scaling. We consider boson sampling where  $N$  independent input optical modes are sent into a linear optical interferometer. The interferometer has  $M$  modes, which can be larger than  $N$ , making  $M - N$  modes at the input vacuum states. As photons interact throughout the interferometer, the quantum state gets transformed according to a unitary matrix describing the interferometer, and photons eventually exit the  $M$  optical modes with non-trivial correlation. For boson sampling, the claim is that this process is hard to simulate for a sufficiently random unitary describing the interferometer.

Formally, the quantum state of  $N$  independent and identical modes can be written as:

$$|\psi_{\text{in}}\rangle = \otimes_{j=1}^N |\psi\rangle_j = \otimes_{j=1}^N \left( \sum_{n=0}^{\infty} c_n \frac{\hat{a}_j^{\dagger n}}{\sqrt{n!}} \right) |0\rangle, \quad (5)$$

where  $\hat{a}_j^{\dagger}$  is the input creation operator for mode  $j$ . The corresponding density operator is

$$\hat{\rho}_{\text{in}} = \otimes_{j=1}^N |\psi\rangle_j \langle \psi|_j = \otimes_{j=1}^N \hat{\rho}_{j,\text{in}}, \quad (6)$$

where the single input mode density operator is

$$\hat{\rho}_{j,\text{in}} = \sum_{n,m=0}^{\infty} c_n c_m^* |n\rangle_j \langle m|_j. \quad (7)$$

The action of an  $M$ -mode beam splitter array is to transform input creation operators:

$$\hat{a}_j^{\dagger} \rightarrow \hat{b}_j^{\dagger} = \sum_{k=1}^M U_{jk} \hat{a}_k^{\dagger}. \quad (8)$$

To study the entanglement entropy between bipartitions separated at the  $l$ th mode, we can define the normalized up and down bipartition creation operators  $\hat{B}_{\text{u},j}^{\dagger}, \hat{B}_{\text{d},j}^{\dagger}$  as

$$\cos \theta_j \hat{B}_{\text{u},j}^{\dagger} = \sum_{k=1}^l U_{jk} \hat{a}_k^{\dagger}, \quad \sin \theta_j \hat{B}_{\text{d},j}^{\dagger} = \sum_{k=l+1}^M U_{jk} \hat{a}_k^{\dagger}, \quad (9)$$

with normalizations

$$\cos^2 \theta_j = \sum_{k=1}^l |U_{jk}|^2, \quad \sin^2 \theta_j = \sum_{k=l+1}^M |U_{jk}|^2. \quad (10)$$

In the collision-free cases where  $M \geq N^2$ , the bipartition creation operators satisfy the canonical commutation relations

$$[\hat{B}_{\text{u},j}, \hat{B}_{\text{u},k}^{\dagger}] = \delta_{jk}, \quad [\hat{B}_{\text{d},j}, \hat{B}_{\text{d},k}^{\dagger}] = \delta_{jk}, \quad (11)$$

$$[\hat{B}_{\text{u},j}, \hat{B}_{\text{d},k}] = 0, \quad [\hat{B}_{\text{u},j}, \hat{B}_{\text{d},k}^{\dagger}] = 0.$$

As a result, one can define the mutually orthogonal bipartition number states

$$\hat{B}_{\text{side},j}^{\dagger k} |0\rangle = \frac{|k\rangle_{\text{side},j}}{\sqrt{k!}}, \text{ side } \in \{\text{u,d}\}. \quad (12)$$

The above formalism, described in [32], allows us to calculate the MPO EE without explicitly constructing the output state given the unitary representing the interferometer. Specifically, the details of the unitary matrix are hidden in the  $|k\rangle_{\text{side},j}$  states constructed to satisfy orthogonality.

In this picture, the action of the unitary is to transform the input basis in the following way:

$$|n\rangle_j \rightarrow \sum_{k_j=0}^n \sqrt{\binom{n}{k_j}} \cos^{k_j} \theta_j \sin^{n-k_j} \theta_j |k_j\rangle_{\text{u},j} |n-k_j\rangle_{\text{d},j}, \quad (13)$$

and therefore

$$\langle k_{\text{u}}, k_{\text{d}} | U | n \rangle = \sqrt{\binom{n}{k_{\text{u}}}} \cos^{k_{\text{u}}} \theta \sin^{k_{\text{d}}} \theta \delta(k_{\text{u}} + k_{\text{d}} - n). \quad (14)$$

If we apply this basis transform due to the unitary to the input lossless density operator, each single mode input density operator in Eq. 6 would transform independently. The full density operator remains a product of input modes in the new basis, and we have

$$\hat{\rho}_{\text{out}} = \otimes_j^N \hat{\rho}_{j,\text{out}}. \quad (15)$$

Although each  $\hat{\rho}_{j,\text{out}}$  can be identified with an input mode  $j$ ,  $\hat{\rho}_{j,\text{out}}$  is no longer a single mode state, and is instead supported over all modes. Each  $\hat{\rho}_{j,\text{out}}$  has some EE because it describes a state over both partitions, and the full system EE is additive in  $j$ . Therefore, the system EE scales linearly with the number of input modes  $N$ , and classical simulation of lossless boson sampling is always inefficient in  $N$ .

We can extend this analysis to lossy cases. Assuming that loss is uniform throughout the interferometer, loss commutes with all linear optical transforms and can be applied to the initial pure state. The basis transform 13 due to the unitary is still independent on  $j$ , and the total output density operator is still in a product form with

$$\hat{\rho}_{j,\text{out}} = U \mathcal{E}_{\text{loss}}(\hat{\rho}_{j,\text{in}}) U^{\dagger}. \quad (16)$$

Therefore, the linear scaling of EE in  $N$  remains, and MPO simulations of lossy boson sampling is also inefficient in  $N$ .

However, as the number of input modes  $N$  increases, the complexity of the interferometer must grow as well in order to maintain reasonable randomness in the interferometer unitary and hardness of classical simulation. As a result, the depth of the interferometer should scale with the  $N$ , which leads to scaling of the transmission rate  $\mu$  in  $N$ . The entanglement entropy for each  $\hat{\rho}_j$  decreases as  $N$  increases, leading to an overall entanglement entropy that grows sublinearly, potentially allowing efficient simulation. To understand the scaling in loss and transmission, consider the Kraus operators corresponding to

the single input state photon loss channel in the limit of small  $\mu$  (from now on we ignore the mode index  $j$ )

$$\hat{\rho}_{\text{lossy}} = \mathcal{E}_{\text{loss}}(\hat{\rho}_{\text{in}}) = \sum_{n_{\text{loss}}=0}^{n_{\text{max}}} K^{(n_{\text{loss}})} \hat{\rho}_{\text{in}} K^{(n_{\text{loss}})\dagger}, \quad (17)$$

$$K^{(n_{\text{loss}})} = \sum_{n_{\text{out}}, n_{\text{in}}=0}^{n_{\text{max}}} K_{n_{\text{out}}, n_{\text{in}}}^{(n_{\text{loss}})} |n_{\text{out}}\rangle \langle n_{\text{in}}| \quad (18)$$

$$K_{n_{\text{out}}, n_{\text{in}}}^{(n_{\text{loss}})} = \begin{cases} \sqrt{\binom{n_{\text{in}}}{n_{\text{out}}}} \mu^{n_{\text{out}}} (1 - \mu)^{n_{\text{loss}}} & \text{if } n_{\text{in}} - n_{\text{out}} = n_{\text{loss}} \\ 0 & \text{otherwise,} \end{cases} \quad (19)$$

where  $K^{(n_{\text{loss}})} \in \mathbb{C}^{n_{\text{max}}+1, n_{\text{max}}+1}$  captures processes that lose  $n_{\text{loss}}$  photons, and we limit the maximum photon number to  $n_{\text{max}}$ . The lossy density operator can be given in the input  $|n\rangle$  basis in index notation:

$$\begin{aligned} \rho_{\text{lossy } m, n} &= \sum_{n_{\text{loss}}=0}^{n_{\text{max}}} \sum_{k, l} K_{m, k}^{(n_{\text{loss}})} \rho_{\text{in } k, l} K_{l, n}^{(n_{\text{loss}})\dagger}, \\ &= \sum_{n_{\text{loss}}=0}^{n_{\text{max}}} O(\mu^{\frac{m}{2}}) \rho_{\text{in } m+n_{\text{loss}}, n+n_{\text{loss}}} O(\mu^{\frac{n}{2}}) \\ &= O(\mu^{\frac{m+n}{2}}), \end{aligned} \quad (20)$$

where the second line is due to the requirement that  $k - m = n_{\text{loss}}$  and  $l - n = n_{\text{loss}}$  from non-zero Kraus operator elements.

We can now apply the basis transform due to the unitary as described in Eq. 13:

$$\begin{aligned} \hat{\rho}_{\text{out}} &= U \hat{\rho}_{\text{lossy}} U^\dagger \\ &= U \left( \sum_{m, n=0}^{n_{\text{max}}} |m\rangle \rho_{\text{lossy } m, n} \langle n| \right) U^\dagger \end{aligned} \quad (21)$$

In index notation in the bipartition number state basis,

$$\begin{aligned} \rho_{\text{out } k_{\text{u}}, k_{\text{d}}; k'_{\text{u}}, k'_{\text{d}}} &= \langle k_{\text{u}}, k_{\text{d}} | \hat{\rho}_{\text{out}} | k'_{\text{u}}, k'_{\text{d}} \rangle \\ &= \sum_{m, n=0}^{n_{\text{max}}} \langle k_{\text{u}}, k_{\text{d}} | U | m \rangle \rho_{\text{lossy } m, n} \langle n | U^\dagger | k'_{\text{u}}, k'_{\text{d}} \rangle. \end{aligned} \quad (22)$$

Substituting Eq. 14 and 20 into the above expression yields

$$\begin{aligned} \rho_{\text{out } k_{\text{u}}, k_{\text{d}}; k'_{\text{u}}, k'_{\text{d}}} &= \sum_{n_{\text{loss}}=0}^{n_{\text{max}}} \rho_{\text{in } k_{\text{u}} + k_{\text{d}} + n_{\text{loss}}, k'_{\text{u}} + k'_{\text{d}} + n_{\text{loss}}} O(\mu^{\frac{k_{\text{u}} + k_{\text{d}} + k'_{\text{u}} + k'_{\text{d}}}{2}}). \end{aligned} \quad (23)$$

To compute the MPO entanglement entropy, we need to vectorize the density operator to obtain  $|\hat{\rho}_{j, \text{out}}\rangle$ , take the outer product to find the corresponding density operator  $|\hat{\rho}_{j, \text{out}}\rangle \langle \hat{\rho}_{j, \text{out}}|$ , take the partial trace over one bipartition to obtain  $\hat{\rho}' = \text{tr}_{\text{u}}(|\hat{\rho}_{j, \text{out}}\rangle \langle \hat{\rho}_{j, \text{out}}|)$ , find its eigenvalues, normalize the eigenvalues (vectorized density operator is no longer of unit trace), and compute the entropy.

Vectorization of the density operator yields:

$$\begin{aligned} \hat{\rho}_{\text{out}} &= \sum_{k_{\text{u}}, k_{\text{d}}, k'_{\text{u}}, k'_{\text{d}}} |k_{\text{u}}, k_{\text{d}}\rangle \rho_{\text{out } k_{\text{u}}, k_{\text{d}}; k'_{\text{u}}, k'_{\text{d}}} \langle k'_{\text{u}}, k'_{\text{d}}| \\ \rightarrow |\hat{\rho}_{\text{out}}\rangle \rangle &= \sum_{k_{\text{u}}, k_{\text{d}}, k'_{\text{u}}, k'_{\text{d}}} \rho_{\text{out } k_{\text{u}}, k_{\text{d}}; k'_{\text{u}}, k'_{\text{d}}} |k_{\text{u}}, k_{\text{d}}; k'_{\text{u}}, k'_{\text{d}}\rangle \\ &= \sum_{K_{\text{u}}, K_{\text{d}}} \rho_{\text{out } K_{\text{u}}, K_{\text{d}}} |K_{\text{u}}, K_{\text{d}}\rangle, \end{aligned} \quad (24)$$

where  $K_{\text{side}}$  is the combined index of  $k_{\text{side}}$  and  $k'_{\text{side}}$ . Taking the partial trace of the density operator of the vectorized state yields

$$\begin{aligned} \rho'_{K_{\text{d}}, \bar{K}_{\text{d}}} &= \sum_{K_{\text{u}}} \rho_{\text{out } K_{\text{u}}, K_{\text{d}}} \rho_{\text{out } K_{\text{u}}, \bar{K}_{\text{d}}}^* \\ &= \sum_{k_{\text{u}}, k'_{\text{u}}} O(\mu^{\frac{k_{\text{u}} + k_{\text{d}} + k'_{\text{u}} + k'_{\text{d}}}{2}}) O(\mu^{\frac{k_{\text{u}} + \bar{k}_{\text{d}} + k'_{\text{u}} + \bar{k}'_{\text{d}}}{2}}) \\ &= O(\mu^{\frac{k_{\text{d}} + k'_{\text{d}} + \bar{k}_{\text{d}} + \bar{k}'_{\text{d}}}{2}}). \end{aligned} \quad (25)$$

where  $\bar{K}$  is the dual of  $K$ , and  $k_{\text{u}}, k'_{\text{u}} = 0$  terms are dominant.

The above analysis is general and independent of the input states. From now on, we will use the fact that the input state is a squeezed state. In GBS,  $\rho_{\text{in } m, n} = 0$  if either  $m$  or  $n$  is odd. Therefore, looking at Eq. 23,  $k_{\text{u}} + k_{\text{d}} + n_{\text{loss}}$  and  $k'_{\text{u}} + k'_{\text{d}} + n_{\text{loss}}$  (or, more concisely,  $k_{\text{u}} + k_{\text{d}}$  and  $k'_{\text{u}} + k'_{\text{d}}$ ) must have the same parity for  $\rho_{\text{in } k_{\text{u}} + k_{\text{d}} + n_{\text{loss}}, k'_{\text{u}} + k'_{\text{d}} + n_{\text{loss}}}$  to be non-zero. This means that we do not have to consider terms like  $\rho_{\text{out } 0, 0; 0, 1}$ ,  $\rho_{\text{out } 1, 0; 0, 0}$ , etc. As a result, no half-integer powers of  $\mu$  occur in any terms of the output density operator  $\hat{\rho}_{\text{out}}$  or the reduced density operator  $\hat{\rho}'$  of the vectorized state.

In this case, it turns out that  $\hat{\rho}'$  has exactly one constant order eigenvalue, no first order eigenvalues, and all other eigenvalues are at least second order. To show this, it is sufficient to find all eigenvalues to the first order. Let us write down the form of  $\hat{\rho}'$  to the first order, with the first row corresponding to  $K_{\text{d}} = k_{\text{d}} = k'_{\text{d}} = 0$  and the first column corresponding to  $\bar{K}_{\text{d}} = \bar{k}_{\text{d}} = \bar{k}'_{\text{d}} = 0$ :

$$\hat{\rho}' = \begin{bmatrix} \hat{\rho}'_{1,1} & \hat{\rho}'_{1,2} & \hat{\rho}'_{1,3} & \cdots \\ \hat{\rho}'_{1,2}^* & 0 & 0 & \vdots \\ \hat{\rho}'_{1,3}^* & 0 & 0 & \vdots \\ \vdots & \cdots & \cdots & \ddots \end{bmatrix}, \quad (26)$$

which has eigenvalues

$$\lambda^2 = \frac{1}{2} \left( \hat{\rho}'_{1,1} \pm \sqrt{\hat{\rho}'_{1,1}^2 + 4 \sum_{n=2}^{(n_{\text{max}}+1)^2} |\hat{\rho}'_{1,n}|^2} \right), \quad (27)$$

and all other eigenvalues are 0. Note that we call the singular values of the Schmidt decompositions  $\lambda$  and the eigenvalues of the reduced density matrices  $\lambda^2$ . However,  $|\hat{\rho}'_{1,n}|^2$  is at least  $O(\mu^2)$ , and the Taylor expansion of the square root will be

dominated by the constant and first order contributions from  $\hat{\rho}'_{1,1}$ . Therefore, the only non-zero first order eigenvalue is  $\lambda_1^2 = \hat{\rho}'_{1,1}$ , which is  $O(1)$ .

The above analysis shows that to the second order, the eigenvalues are

$$\{a + b\mu + c\mu^2, O(\mu^2), O(\mu^2), O(\mu^2), \dots\}. \quad (28)$$

After normalization of the eigenvalues, the entropy contribution due to  $\lambda_1^2$  is

$$\begin{aligned} & -\frac{a + b\mu + c_1\mu^2}{C} \log \frac{a + b\mu + c_1\mu^2}{C} \\ & = \frac{(d - c_1)\mu^2}{a \ln 2} + O(\mu^3) = O(\mu^2), \end{aligned} \quad (29)$$

where  $c_i$  is the second order coefficient of  $\lambda_i^2$ ,  $d = \sum_i c_i$ , and  $C = a + b\mu + d\mu^2$  is the normalization that must be treated explicitly and not as a constant. Contribution of other eigenvalues are

$$-\frac{c_i\mu^2}{C} \log_2 \frac{c_i\mu^2}{C} = O(-\mu^2 \log_2 \mu). \quad (30)$$

Overall, the entanglement entropy scales as  $O(\mu^2 \log \mu)$ . We would like to understand the scaling of the MPO EE under various loss scalings with the number of input optical modes. Generically, one can consider the situation where the number of surviving photons scales as  $N_{\text{out}} \propto N^\gamma$ , making the transmission rate  $\mu = \beta N^\gamma / N$ . Since the total entanglement entropy is the sum of all  $N$  input modes, we obtain

$$\begin{aligned} S_1(|\hat{\rho}\rangle\rangle) &= O\left(N \left(\frac{\beta N^\gamma}{N}\right)^2 \log_2 \left(\frac{\beta N^\gamma}{N}\right)\right) \\ &= O(N^{2\gamma-1} \log_2 N). \end{aligned} \quad (31)$$

Similarly, for the Rényi entropy, contribution from a single  $\hat{\rho}_{j,\text{out}}$  is

$$\begin{aligned} & \frac{1}{1-\alpha} \log_2 \left[ \left( \frac{a + b\mu + c_1\mu^2}{C} \right)^\alpha + \sum_{i \neq 1} \left( \frac{c_i\mu^2}{C} \right)^\alpha \right] \\ & \approx \frac{1}{(1-\alpha) \ln 2} \left( -\frac{d - c_1}{a} \alpha \mu^2 + \frac{1}{a} \sum_{i \neq 1} c_i^\alpha \mu^{2\alpha} \right). \end{aligned} \quad (32)$$

Therefore, for  $\alpha < 1$ , the second term dominates, and we have the familiar

$$S_\alpha = O(N^{1-2(1-\gamma)\alpha}). \quad (33)$$

Similarly, for  $\alpha > 1$ , the first term dominates, and we have

$$S_\alpha = O\left(\frac{\alpha}{1-\alpha} N^{2\gamma-1}\right). \quad (34)$$

## B. Numerical asymptotic estimates of the entanglement entropy

For our numerical estimates of GBS operator EE, we use the input wavefunction for a single squeezed mode

$$|\psi_{\text{in}}\rangle = \frac{1}{\sqrt{\cosh r}} \sum_{n=0}^{n_{\text{max}}/2} \frac{\tanh^n r}{2^n n!} \hat{a}^{\dagger 2n} |0\rangle, \quad (35)$$

follow the steps discussed above to compute the single mode EE contribution, and multiply by the number of input modes. The coefficients  $\cos \theta_j, \sin \theta_j$  related to the unitary can also be simply approximated as  $1/\sqrt{2}$  in the asymptotic limit of large  $M$  if  $l$  is chosen to be  $M/2$  as can be seen from Eq. 10. This choice of bipartition should produce the largest MPO EE.

Specifically, we examine photon survival scaling  $N_{\text{out}} \propto N^\gamma$  with  $\gamma = \frac{1}{4}, \frac{1}{2}, 1$ . To make a fair comparison against SPBS, the squeezing parameter is fixed at  $r = 0.88$ , which averages to approximately one photon per squeezed mode.

Fig. 1 shows the asymptotic estimates with  $n_{\text{max}} = 8$  for large system sizes. Similar to what is observed in SPBS simulations, GBS shows MPO EE reduction when the loss is sufficiently high for  $\gamma = \frac{1}{4}$ , logarithmic scaling for  $\gamma = \frac{1}{2}$ , and linear scaling for  $\gamma = 1$ . A similar linear increase in MPO EE with  $\beta$  is also observed in all three cases. Further, we also show the numerical convergence of our asymptotic MPO EE estimates by increasing the cut-off of the initial maximum photon number  $n_{\text{max}}$  for the squeezed states.

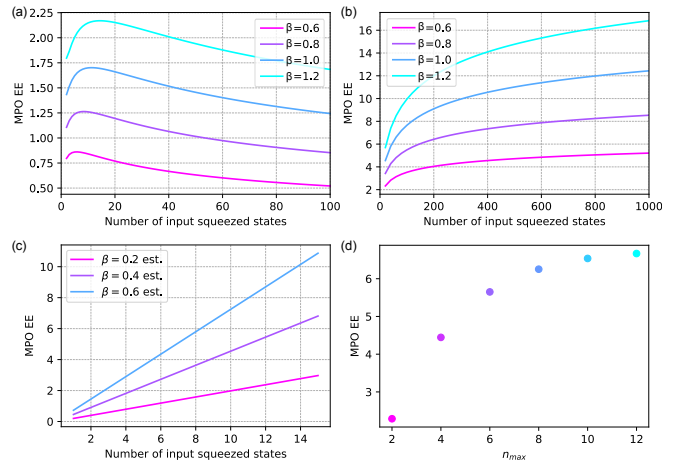


Figure 1. Operator entanglement entropy vs. the number of input squeezed modes for different photon survival scaling  $N_{\text{out}} = \beta N^\gamma$  at  $r = 0.88$ . (a)  $\gamma = \frac{1}{4}$ . (b)  $\gamma = \frac{1}{2}$ . (c)  $\gamma = 1$ . (d) Convergence of MPO EE with increasing  $n_{\text{max}}$  for  $N = 50, \beta = 1, \gamma = \frac{1}{2}, r = 0.88$ .

## C. MPO simulations

We further conduct full MPO simulations of GBS and numerically calculate the MPO EE. The full simulations and asymptotic forms agree quantitatively, as shown in Fig. 2.

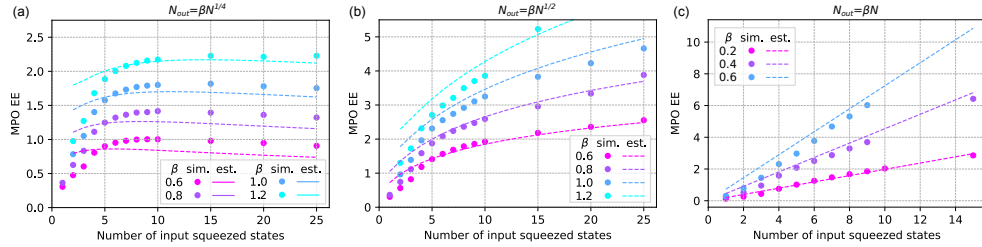


Figure 2. Operator entanglement entropy vs. the number of input squeezed modes for different photon survival scaling  $N_{\text{out}} = \beta N^\gamma$  at  $r = 0.88$ . Details of experiment configurations can be found in Methods. (a)  $\gamma = \frac{1}{4}$ . (b)  $\gamma = \frac{1}{2}$ . (c)  $\gamma = 1$ . Dots are results obtained from full simulations using  $U(1)$  symmetry. Dashed lines are estimates using asymptotic assumptions.

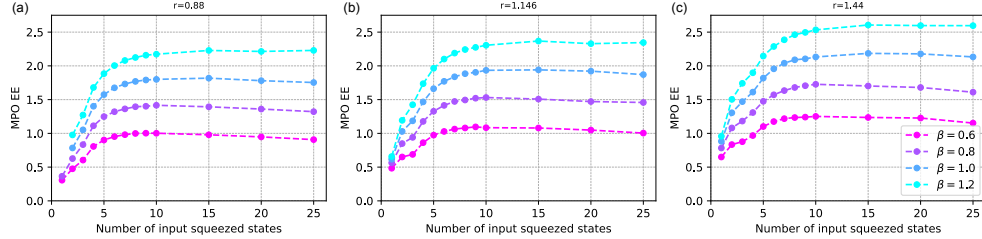


Figure 3. Operator entanglement entropy vs. the number of input squeezed modes for different squeezing parameters  $r$ . (a)  $r = 0.88$ , averaging approximately 1 photon per mode. (b)  $r = 1.146$ , averaging approximately 2 photons per mode. (b)  $r = 1.44$ , averaging approximately 4 photons per mode.

However, we observe that the quality of agreement is poor when MPO EE is small such as in many  $\gamma = \frac{1}{4}$  data points when the number of input squeezed states  $N$  is small. In the regime of small MPO EE but large  $N$ , we attribute the disagreement to the formal differences between regular MPOs and MPOs in a  $U(1)$  symmetric form. This is easy to see as even a product state can have non-zero  $U(1)$  symmetric MPO EE simply due to the existence of different charges. For small  $N$ , we expect the quality of the approximation to be poor because we are no longer in the asymptotic limit. Further disagreement can also be attributed to the fact that the  $U(1)$  symmetric full simulations are limited by the bond dimension. We ensure that all plotted data points are simulated to  $1 - \text{Tr}(\hat{\rho}) < 0.1$ , which previous work established as a good proxy to the total variation error that is computationally lightweight.

Lastly, we investigate the effect of squeezing on MPO EE with our full  $U(1)$  symmetric simulations. We choose to investigate  $\gamma = \frac{1}{4}$  for easier simulation. Fig. 3 shows an increase in MPO EE with increasing squeezing parameter  $r$ . It is important to note that the average number of output photons scales with the average number of input photons  $N$ , not the number of squeezed states. This means that for the same number of input squeezed states and  $\beta$ , a higher squeezing parameter has a higher loss. Increasing the average number of photons per squeezed mode from 1 to 2 and 4 only moderately increases the MPO EE compared to increasing  $N$ . This observation is similar to the previous finding for Fock state boson sampling: if the number of input modes stays the same and the number of photons per mode increases, the MPO EE grows slowly and can be efficiently simulated [32].

Our numerical findings on the MPO EE growth for different loss scalings have complexity implications, but there is a lack of rigorous correspondence between MPO EE and simulation time. Although we can formally perform Schmidt decomposition on the vectorized mixed state and identify the singular values with  $\lambda$ 's in the MPO representation, the interpretation of entanglement becomes murkier because of the incorporation of classical correlation in the expression. Further, suitable truncation of the singular values ensures that the 2-norm between the approximate vectorized mixed state and the ideal vectorized mixed state is controlled. However, the bound on the trace distance between the density operators is larger by a factor of the dimension of the Hilbert space. Therefore, when the MPO EE decreases as the system size increases, the required bond dimension to bound the 2-norm decreases, but the required bond dimension to bound the trace distance may still increase.

To make the statement on simulation complexity more rigorous, we validate the bond dimension growth explicitly. This is helpful in particular because the computational complexity is cubic in the bond dimension, both due to SVD and matrix multiplication. We show in Fig. 4 the growth of bond dimension in the system size for fixed accuracy of  $1 - \text{Tr}(\hat{\rho}) = 0.02$ . It is clear that constant loss leads to exponential growth in the bond dimension. In higher loss cases, growth is much more moderate and appears sub-exponential. We also validate that increasing the bond dimension efficiently reduces the simulation error. We choose three experiments and simulated them with different bond dimensions.

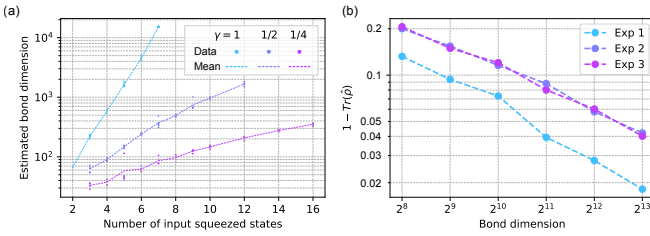


Figure 4. Analysis of bond dimension, system size, and error. Details can be found in Methods. (a) Bond dimension needed to reach accuracy  $1 - \text{Tr}(\hat{\rho}) = 0.02$  vs. the number of input squeezed modes photon survival scaling  $N_{\text{out}} = 0.4N^{\gamma}$  at  $r = 0.88$ . Dots are individual estimates of the bond dimension obtained from full simulations using  $U(1)$  symmetry. Dashed lines are the means. (b) Reduction in  $1 - \text{Tr}(\hat{\rho})$  error as bond dimension increases for three different experimental configurations.

#### IV. DISCUSSION

We show analytically that the matrix product operator entanglement entropy of boson sampling scales logarithmically under high loss, which we numerically verify using  $U(1)$  symmetric tensor networks. We also numerically observe that increasing the photon number by squeezing has little impact compared to increasing the number of input squeezed modes. The computational complexity is also directly studied by calculating the bond dimension. This extends the previous entanglement entropy results for single photon boson sampling to the more experimentally relevant Gaussian boson sampling, and extends the efficient simulation results using classical state approximation algorithms to an algorithm with controllable error, a necessary condition for simulating intermediate-size experiments with practical transmission rates. As a result, our analysis is more relevant to current quantum supremacy boson sampling experiments.

Although the MPO formalism intrinsically assumes a 1D architecture of the interferometer, the fact that we are simulating Haar random unitaries means that our findings are architecture independent. However, if we want to simulate high dimensional low depth systems that are not Haar random [28, 54], one potential direction to move forward is to adopt more exotic tensor networks such as projected entanglement pair states (PEPS), and  $U(1)$  symmetric forms of generic tensor networks can be constructed in principle [52].

#### DATA AVAILABILITY

Data used to generate the figures are available upon request from the authors.

#### CODE AVAILABILITY

The code used to generate the data and figures is available in the GitHub repository <https://github.com/>

sss441803/BosonSampling.

#### ACKNOWLEDGEMENTS

This research used the resources of the Argonne Leadership Computing Facility, which is a U.S. Department of Energy (DOE) Office of Science User Facility supported under Contract DE-AC02-06CH11357. Y.A. acknowledges support from the Office of Science, U.S. Department of Energy, under contract DE-AC02-06CH11357 at Argonne National Laboratory and Defense Advanced Research Projects Agency (DARPA) under Contract No. HR001120C0068. L. J. acknowledges support from the the ARO(W911NF-23-1-0077), ARO MURI (W911NF-21-1-0325), AFOSR MURI (FA9550-19-1-0399, FA9550-21-1-0209), AFRL (FA8649-21-P-0781), DoE Q-NEXT, NSF (OMA-1936118, ERC-1941583, OMA-2137642), NTT Research, and the Packard Foundation (2020-71479). J.L. is supported in part by International Business Machines (IBM) Quantum through the Chicago Quantum Exchange, and the Pritzker School of Molecular Engineering at the University of Chicago through AFOSR MURI (FA9550-21-1-0209). M.L. acknowledges support from DOE Q-NEXT. C.O. acknowledges support from the ARO (Grants No. W911NF-18-1-0020 and No. W911NF-18-1-0212), ARO MURI (Grant No. W911NF-16-1-0349), AFOSR MURI (Grants No. FA9550-19-1-0399 and No. FA9550-21-1-0209), DOE Q-NEXT, NSF (Grants No. EFMA-1640959, No. OMA-1936118, No. EEC-1941583), NTT Research, and the Packard Foundation (2013-39273).

#### V. COMPETING INTERESTS

The authors declare no competing financial or non-financial interests.

#### VI. AUTHOR CONTRIBUTIONS

M.L. developed the majority of the software, performed all numerical simulations and theoretical derivations, and wrote the majority of the manuscript. C.O. provided the original CPU implementation, developed the MPO initialization scheme, performed preliminary theoretical work, and contributed significantly to manuscript editing. All other authors contributed novel ideas, provided numerous scientific and writing improvements about the paper, and participated in discussions that shaped the project in a substantial manner and the understanding of its broader impact.

#### APPENDIX A: TECHNICAL DETAILS

We carry out our GPU numerical simulations using the Polaris system at the Argonne Leadership Computing Facility (ALCF). Each node has a single 2.8 GHz AMD EPYC Milan 7543P 32-core CPU with 512 GB of DDR4 RAM and four

Nvidia A100 GPUs connected via NVLink. We perform our CPU numerical simulations using the Bebop system at ALCF. Each node has a single 2.10 GHz Intel Xeon E5-2695v4 32-core CPU with 128GB of DDR4 RAM.

All full  $U(1)$  symmetric MPO simulations have  $M = \max(20, 4N)$  modes, and the local Hilbert space dimension  $d$  is chosen such that  $< 1\%$  of the probability is truncated. Because the left-most charge is the sum of all photons, the required  $d$  is higher for higher squeezing parameters  $r$  and higher numbers of input squeezed states. Global Haar random interferometers are used and constructed using an  $M$ -layer array [55].

For Fig. 2 and 3, we simulate the system until there is no MPO EE increase for at least 10 layers. This is reasonable since we only care about the maximum MPO EE throughout simulation which captures the computational cost, and the MPO EE generically increases as more depths are simulated until saturation, after which the MPO EE decreases slowly. All data points of MPO EE are obtained by only a single experiment, as we observe that no significant noise is present

in our results because we only extract the maximum. We ensure that all plotted data points are simulated to  $1 - \text{Tr}(\hat{\rho}) < 0.1$ , which previous work established as a good proxy to the total variation error that is computationally lightweight. The largest simulation is for linear scaling simulations with  $d = 18$ ,  $\beta = 0.4$ ,  $N = 15$ ,  $M = 60$ ,  $\chi = 16384$  ran on 10 Polaris nodes with 40 GPUs in total.

For Fig. 4, the full depth of the interferometer is simulated. This is because simulating each layer produces additional error, and therefore affects the required bond dimension. For each configuration in Fig. 4 a, the bond dimension starts with a small value and doubles if the error exceeds 0.02. Once the bond dimension is large enough to exceed the desired accuracy, the bond dimension is refined a few more times to obtain a more precise estimate. For linear scaling and 7 input squeezed states, the simulation is expensive and we verified that setting  $\chi = 15296$  produced  $1 - \text{Tr}(\hat{\rho}) = 0.020, 0.022, 0.021, 0.021, 0.019$  across 5 different experiments and used 15296 as the estimated bond dimension. The three experiments for Fig. 4 b are  $M = 10, 15, 20$  and  $\mu = 0.2, 0.15, 0.1$  respectively, and each data point is obtained from one simulation.

---

[1] P. W. Shor, “Algorithms for quantum computation: discrete logarithms and factoring,” in *Proceedings 35th annual symposium on foundations of computer science* (Ieee, 1994) pp. 124–134.

[2] Lov K. Grover, “A fast quantum mechanical algorithm for database search,” in *Proceedings of the Twenty-Eighth Annual ACM Symposium on Theory of Computing*, STOC ’96 (Association for Computing Machinery, New York, NY, USA, 1996) p. 212–219.

[3] Aram W. Harrow, Avinatan Hassidim, and Seth Lloyd, “Quantum algorithm for linear systems of equations,” *Phys. Rev. Lett.* **103**, 150502 (2009).

[4] D. W. Berry, G. Ahokas, R. Cleve, and B. C. Sanders, “Efficient quantum algorithms for simulating sparse hamiltonians,” *Commun. Math. Phys.* **270**, 359–371 (2007).

[5] Dominic W. Berry, Andrew M. Childs, Richard Cleve, Robin Kothari, and Rolando D. Somma, “Exponential improvement in precision for simulating sparse hamiltonians,” in *Proceedings of the Forty-Sixth Annual ACM Symposium on Theory of Computing*, STOC ’14 (Association for Computing Machinery, New York, NY, USA, 2014) p. 283–292.

[6] A.M. Childs, “On the relationship between continuous- and discrete-time quantum walk,” *Commun. Math. Phys.* **294**, 581–603 (2010).

[7] Guang Hao Low and Isaac L. Chuang, “Optimal hamiltonian simulation by quantum signal processing,” *Phys. Rev. Lett.* **118**, 010501 (2017).

[8] Yuri Alexeev *et al.*, “Quantum computer systems for scientific discovery,” *PRX Quantum* **2** (2021), 10.1103/prxquantum.2.017001.

[9] S. Aaronson and A. Arkhipov, “The computational complexity of linear optics,” in *Proceedings of the forty-third annual ACM symposium on Theory of computing* (2011) pp. 333–342.

[10] M. A. Broome, A. Fedrizzi, S. Rahimi-Keshari, J. Dove, S. Aaronson, T. C. Ralph, and A. G. White, “Photonic boson sampling in a tunable circuit,” *Science* **339**, 794–798 (2013).

[11] J. B. Spring, B. J. Metcalf, P. C. Humphreys, W. S. Kolthammer, X.-M. Jin, M. Barbieri, A. Datta, N. Thomas-Peter, N. K. Langford, D. Kundys, *et al.*, “Boson sampling on a photonic chip,” *Science* **339**, 798–801 (2013).

[12] M. Tillmann, B. Dakić, R. Heilmann, S. Nolte, A. Szameit, and P. Walther, “Experimental boson sampling,” *Nat. Photonics* **7**, 540–544 (2013).

[13] A. Crespi, R. Osellame, R. Ramponi, D. J. Brod, E. F. Galvão, N. Spagnolo, C. Vitelli, E. Maiorino, P. Mataloni, and F. Sciarrino, “Integrated multimode interferometers with arbitrary designs for photonic boson sampling,” *Nat. Photonics* **7**, 545–549 (2013).

[14] N. Spagnolo, C. Vitelli, M. Bentivegna, D. J. Brod, A. Crespi, F. Flamini, S. Giacomini, G. Milani, R. Ramponi, P. Mataloni, *et al.*, “Experimental validation of photonic boson sampling,” *Nat. Photonics* **8**, 615–620 (2014).

[15] J. Carolan, J. D. A. Meinecke, P. J. Shadbolt, N. J. Russell, N. Ismail, K. Wörhoff, T. Rudolph, M. G. Thompson, J. L. O’Brien, J. C. F. Matthews, *et al.*, “On the experimental verification of quantum complexity in linear optics,” *Nat. Photonics* **8**, 621–626 (2014).

[16] J. Carolan, C. Harrold, C. Sparrow, E. Martín-López, N. J. Russell, J. W. Silverstone, P. J. Shadbolt, N. Matsuda, M. Oguma, M. Itoh, *et al.*, “Universal linear optics,” *Science* **349**, 711–716 (2015).

[17] M. Bentivegna, N. Spagnolo, C. Vitelli, F. Flamini, N. Vigianiello, L. Latmiral, P. Mataloni, D. J. Brod, E. F. Galvão, A. Crespi, *et al.*, “Experimental scattershot boson sampling,” *Sci. Adv.* **1**, e1400255 (2015).

[18] H.-S. Zhong *et al.*, “12-photon entanglement and scalable scattershot boson sampling with optimal entangled-photon pairs from parametric down-conversion,” *Phys. Rev. Lett.* **121**, 250505 (2018).

[19] H.-S. Zhong *et al.*, “Experimental Gaussian boson sampling,” *Science Bulletin* **64**, 511–515 (2019).

[20] S. Paesani, Y. Ding, R. Santagati, L. Chakhmakhchyan, C. Vigliar, K. Rottwitt, L. K. Oxenløwe, J. Wang, M. G. Thompson, and A. Laing, “Generation and sampling of quantum states of light in a silicon chip,” *Nat. Phys.* **15**, 925–929 (2019).

[21] Y. He, X. Ding, Z.-E. Su, H.-L. Huang, J. Qin, C. Wang, S. Un-sleber, C. Chen, H. Wang, Y.-M. He, *et al.*, “Time-bin-encoded boson sampling with a single-photon device,” *Phys. Rev. Lett.* **118**, 190501 (2017).

[22] J. C. Loredo, M. A. Broome, P. Hilaire, O. Gazzano, I. Sagnes, A. Lemaitre, M. P. Almeida, P. Senellart, and A. G. White, “Boson sampling with single-photon fock states from a bright solid-state source,” *Phys. Rev. Lett.* **118**, 130503 (2017).

[23] H. Wang, Y. He, Y.-H. Li, Z.-E. Su, B. Li, H.-L. Huang, X. Ding, M.-C. Chen, C. Liu, J. Qin, *et al.*, “High-efficiency multiphoton boson sampling,” *Nat. Photonics* **11**, 361–365 (2017).

[24] H. Wang, W. Li, X. Jiang, Y.-M. He, Y.-H. Li, X. Ding, M.-C. Chen, J. Qin, C.-Z. Peng, C. Schneider, *et al.*, “Toward scalable boson sampling with photon loss,” *Phys. Rev. Lett.* **120**, 230502 (2018).

[25] H. Wang, J. Qin, X. Ding, M.-C. Chen, S. Chen, X. You, Y.-M. He, X. Jiang, L. You, Z. Wang, *et al.*, “Boson sampling with 20 input photons and a 60-mode interferometer in a  $10^{14}$ -dimensional hilbert space,” *Phys. Rev. Lett.* **123**, 250503 (2019).

[26] Han-Sen Zhong *et al.*, “Quantum computational advantage using photons,” *Science* (2020), 10.1126/science.abe8770.

[27] Han-Sen Zhong *et al.*, “Phase-programmable gaussian boson sampling using stimulated squeezed light,” *Phys. Rev. Lett.* **127**, 180502 (2021).

[28] L. S. Madsen *et al.*, “Quantum computational advantage with a programmable photonic processor,” *Nature* **606**, 75–81 (2022).

[29] Dorit Aharonov, Michael Ben-Or, Russell Impagliazzo, and Noam Nisan, “Limitations of noisy reversible computation,” arXiv preprint quant-ph/9611028 (1996).

[30] K. Noh, L. Jiang, and B. Fefferman, “Efficient classical simulation of noisy random quantum circuits in one dimension,” *Quantum* **4**, 318 (2020).

[31] Meng Zhang, Chao Wang, Shaojun Dong, Hao Zhang, Yongjian Han, and Lixin He, “Entanglement entropy scaling of noisy random quantum circuits in two dimensions,” arXiv preprint arXiv:2205.13999 (2022).

[32] Changhun Oh, Kyungjoo Noh, Bill Fefferman, and Liang Jiang, “Classical simulation of lossy boson sampling using matrix product operators,” *Phys. Rev. A* **104**, 022407 (2021).

[33] Frank Arute *et al.*, “Quantum supremacy using a programmable superconducting processor,” *Nature* **574**, 505–510 (2019).

[34] Dorit Aharonov, Xun Gao, Zeph Landau, Yunchao Liu, and Umesh Vazirani, “A polynomial-time classical algorithm for noisy random circuit sampling,” arXiv preprint arXiv:2211.03999 (2022).

[35] Changhun Oh, Liang Jiang, and Bill Fefferman, “On classical simulation algorithms for noisy boson sampling,” arXiv preprint arXiv:2301.11532 (2023).

[36] M. Oszmaniec and D. J. Brod, “Classical simulation of photonic linear optics with lost particles,” *New J. Phys.* **20**, 092002 (2018).

[37] R. García-Patrón, J. J. Renema, and V. Shchesnovich, “Simulating boson sampling in lossy architectures,” *Quantum* **3**, 169 (2019).

[38] J. Renema, V. Shchesnovich, and R. García-Patrón, “Classical simulability of noisy boson sampling,” arXiv preprint arXiv:1809.01953 (2018).

[39] Haoyu Qi, Daniel J. Brod, Nicolás Quesada, and Raúl García-Patrón, “Regimes of classical simulability for noisy Gaussian boson sampling,” *Phys. Rev. Lett.* **124**, 100502 (2020).

[40] Malte C Tichy, “Sampling of partially distinguishable bosons and the relation to the multidimensional permanent,” *Physical Review A* **91**, 022316 (2015).

[41] Jelmer J Renema, Adrian Menssen, William R Clements, Gil Triginer, William S Kolthammer, and Ian A Walmsley, “Efficient classical algorithm for boson sampling with partially distinguishable photons,” *Physical review letters* **120**, 220502 (2018).

[42] Valery S Shchesnovich, “Noise in boson sampling and the threshold of efficient classical simulability,” *Physical Review A* **100**, 012340 (2019).

[43] Alexandra E Moylett, Raúl García-Patrón, Jelmer J Renema, and Peter S Turner, “Classically simulating near-term partially-distinguishable and lossy boson sampling,” *Quantum Science and Technology* **5**, 015001 (2019).

[44] A. P. Lund, A. Laing, S. Rahimi-Keshari, T. Rudolph, J. L. O’Brien, and T. C. Ralph, “Boson sampling from a gaussian state,” *Phys. Rev. Lett.* **113**, 100502 (2014).

[45] Sonja Barkhofen, Tim J. Bartley, Linda Sansoni, Regina Kruse, Craig S. Hamilton, Igor Jex, and Christine Silberhorn, “Driven boson sampling,” *Phys. Rev. Lett.* **118**, 020502 (2017).

[46] L. Chakhmakhchyan and N. J. Cerf, “Boson sampling with gaussian measurements,” *Phys. Rev. A* **96**, 032326 (2017).

[47] C. S. Hamilton, R. Kruse, L. Sansoni, S. Barkhofen, C. Silberhorn, and I. Jex, “Gaussian boson sampling,” *Phys. Rev. Lett.* **119**, 170501 (2017).

[48] Regina Kruse, Craig S. Hamilton, Linda Sansoni, Sonja Barkhofen, Christine Silberhorn, and Igor Jex, “Detailed study of gaussian boson sampling,” *Phys. Rev. A* **100**, 032326 (2019).

[49] Yu-Hao Deng *et al.*, “Gaussian boson sampling with pseudo-photon-number resolving detectors and quantum computational advantage,” arXiv preprint arXiv:2304.12240 (2023).

[50] Minzhao Liu, Changhun Oh, Junyu Liu, Liang Jiang, and Yuri Alexeev, “Supercomputing tensor networks for  $U(1)$  symmetric quantum many-body systems,” arXiv preprint arXiv:2303.11409 (2023).

[51] H.-L. Huang, W.-S. Bao, and C. Guo, “Simulating the dynamics of single photons in boson sampling devices with matrix product states,” *Phys. Rev. A* **100**, 032305 (2019).

[52] S. Singh, R. N. C. Pfeifer, and G. Vidal, “Tensor network states and algorithms in the presence of a global  $U(1)$  symmetry,” *Phys. Rev. B* **83**, 115125 (2011).

[53] C. Guo and D. Poletti, “Matrix product states with adaptive global symmetries,” *Phys. Rev. B* **100**, 134304 (2019).

[54] Abhinav Deshpande *et al.*, “Quantum computational advantage via high-dimensional gaussian boson sampling,” *Science Advances* **8**, eabi7894 (2022).

[55] Nicholas J Russell, Levon Chakhmakhchyan, Jeremy L O’Brien, and Anthony Laing, “Direct dialling of haar random unitary matrices,” *New Journal of Physics* **19**, 033007 (2017).